

## Calcium Channel Blocker Verapamil Enhances Endoplasmic Reticulum Stress and Cell Death Induced by Proteasome Inhibition in Myeloma Cells<sup>1,2</sup>

Silke Meister<sup>\*</sup>, Benjamin Frey<sup>†</sup>,  
Veronika R. Lang<sup>\*</sup>, Udo S. Gaipl<sup>†</sup>,  
Georg Schett<sup>‡</sup>, Ursula Schlötzer-Schrehardt<sup>§</sup>  
and Reinhard E. Voll<sup>\*,‡</sup>

<sup>\*</sup>IZKF N2, Nikolaus-Fiebiger-Center of Molecular Medicine, University of Erlangen-Nuremberg, Erlangen, Germany; <sup>†</sup>Department of Radiation Oncology, University of Erlangen-Nuremberg, Erlangen, Germany; <sup>‡</sup>Department for Internal Medicine 3 and Institute for Clinical Immunology, University of Erlangen-Nuremberg, Erlangen, Germany; <sup>§</sup>Department of Ophthalmology, University of Erlangen-Nuremberg, Erlangen, Germany

### Abstract

The proteasome inhibitor bortezomib is clinically approved for the treatment of multiple myeloma. However, long-term remissions are difficult to achieve, and myeloma cells often develop secondary resistance to proteasome inhibitors. We recently demonstrated that the extraordinary sensitivity of myeloma cells toward bortezomib is dependent on their extensive immunoglobulin synthesis, thereby triggering the terminal unfolded protein response (UPR). Here, we investigated whether verapamil, an inhibitor of the multidrug resistance (MDR) gene product, can enhance the cytotoxicity of bortezomib. The combination of bortezomib and verapamil synergistically decreased the viability of myeloma cells by inducing cell death. Importantly, bortezomib-mediated activation of major UPR components was enhanced by verapamil. The combination of bortezomib and verapamil resulted in caspase activation followed by poly(ADP-ribose) polymerase cleavage, whereas nuclear factor  $\kappa$ B (NF- $\kappa$ B) activity declined in myeloma cells. Also, we found reduced immunoglobulin G secretion along with increased amounts of ubiquitinated proteins within insoluble fractions of myeloma cells when using the combination treatment. Verapamil markedly induced reactive oxygen species production and autophagic-like processes. Furthermore, verapamil decreased MDR1 expression. We conclude that verapamil increased the anti-myeloma effect of bortezomib by enhancing ER stress signals along with NF- $\kappa$ B inhibition, leading to cell death. Thus, the combination of bortezomib with verapamil may improve the efficacy of proteasome inhibitory therapy.

*Neoplasia (2010) 12, 550–561*

### Introduction

Multiple myeloma, a virtually incurable plasma cell neoplasia, is characterized by the production of large amounts of monoclonal immunoglobulins and accounts for approximately 10% of all hematologic cancers [1]. Existing therapeutic strategies such as high-dose chemotherapy followed by hematopoietic stem cell transplantation prolong survival of multiple myeloma patients but rarely induce long-lasting complete remissions. These treatments are also associated with severe adverse effects [2].

The proteasome inhibitor bortezomib (Velcade) markedly improved the treatment options for patients with relapsed multiple myeloma by inducing apoptosis in myeloma cells [3]. The dipeptidyl boronic acid derivative bortezomib is a highly selective and reversible inhibitor of the

Abbreviations: ER, endoplasmic reticulum; I $\kappa$ B, inhibitor of kappa B; MDR, multidrug resistance; NF- $\kappa$ B, nuclear factor kappa B; P-gp, p-glycoprotein; ROS, reactive oxygen species; UPR, unfolded protein response

Address all correspondence to: Dr. Reinhard Voll, Internal Medicine 3 and Institute for Clinical Immunology, Nikolaus-Fiebiger-Center of Molecular Medicine, Glueckstrasse 6, 91054 Erlangen, Germany. E-mail: rvoll@molmed.uni-erlangen.de

<sup>1</sup>This work was supported by the Interdisciplinary Center for Clinical Research project no. N2; German Research Society (DFG) Collaborative Research Centers SFB 643 project B3 (R.V.) and FOR832 (VO 673/3-1), the ELAN fond (08.03.12.1) of the University Erlangen-Nuremberg, Germany, and the Doktor Robert Pflieger Foundation, Bamberg, Germany, and the Bavarian Immunotherapy Network (Bay ImmuNet) to R. V.

<sup>2</sup>This article refers to supplementary materials, which are designated by Figures W1 to W4 and are available online at [www.neoplasia.com](http://www.neoplasia.com).

Received 29 January 2010; Revised 5 May 2010; Accepted 7 May 2010

Copyright © 2010 Neoplasia Press, Inc. All rights reserved 1522-8002/10/\$25.00  
DOI 10.1593/neo.10228

26S proteasome, a multienzyme complex present in all eukaryotic cells. The 26S proteasome degrades supernumerous, defective, or misfolded proteins, which are targeted for proteasomal degradation by polyubiquitinylation. In addition, it plays a fundamental role in cellular homeostasis as a critical regulator of cell proliferation and apoptosis [4,5].

The antitumor effect of bortezomib has been demonstrated *in vitro* and *in vivo* for various types of cancers. Myeloma cells seem to be exceptionally sensitive. Even the growth of chemotherapy-resistant myeloma cell lines was inhibited by bortezomib treatment [6]. Bortezomib exerts its effect through multiple pathways that target both the tumor cell and its environment. The cytotoxic effect of bortezomib seems to be partially due to the inhibition of the antiapoptotic transcription factor nuclear factor  $\kappa$ B (NF- $\kappa$ B). Bortezomib stabilizes endogenous inhibitor of kappa B alpha (I $\kappa$ B $\alpha$ ) that sequesters NF- $\kappa$ B in the cytoplasm and prevents transcriptional activation of NF- $\kappa$ B target genes [7].

Importantly, we and others demonstrated that bortezomib-induced apoptosis is caused by excessive endoplasmic reticulum (ER) stress, activating the terminal unfolded protein response (UPR), especially in cells with extensive synthesis of secretory proteins [8–11].

The UPR is a signaling pathway from the ER to the nucleus triggered by the accumulation of misfolded proteins in the ER lumen and is essential for plasma cell differentiation and survival. The UPR includes three mechanisms to handle the vast increase of unfolded proteins: transcriptional induction of target genes enhancing protein folding, general translational repression, and ER-associated degradation to eliminate misfolded proteins. However, overwhelming ER stress activates the terminal UPR, leading to apoptosis [12,13].

Some myeloma patients are resistant or become refractory to ongoing bortezomib treatment [14]. To improve the efficacy of proteasome inhibitor-based treatments and to overcome primary and secondary resistance, drugs augmenting the antitumor properties of bortezomib in myeloma cells are required. We identified the L-type calcium channel antagonist verapamil (Isoptin; Abbott, Wiesbaden, Germany), clinically used for the treatment of cardiac arrhythmias, hypertension, and, most recently, for cluster headaches, as a promising combination partner with bortezomib. The phenylalkylamine derivative verapamil potently inhibits the influx of calcium ions into cells [15]. Further, in drug-resistant leukemic cell lines, verapamil interfered with the multidrug resistance (MDR)-based drug elimination by decreasing P-glycoprotein (P-gp) expression [16]. In this study, we observed that verapamil enhanced the proapoptotic effect of bortezomib. Increased cell death was associated with induction of terminal UPR and autophagy; however, a causal link and the molecular mechanisms require further investigation.

## Materials and Methods

### Antibodies

For immunoblot analysis, the following primary antibodies were used: mouse monoclonal anti-GRP78 (BiP), rabbit polyclonal anti-GRP94, and mouse monoclonal anti-poly(ADP-ribose) polymerase (PARP; BD Pharmingen, Heidelberg, Germany); mouse monoclonal anti-Bcl-2, rabbit polyclonal anti-Bax, rabbit polyclonal anti-Bim, mouse monoclonal anti-caspase 9, rabbit polyclonal anti-CHOP, rabbit polyclonal anti-p-eIF2 $\alpha$ , mouse monoclonal anti-Hsp70, rabbit polyclonal anti-inositol-requiring transmembrane kinase/endonuclease 1 $\alpha$  (IRE1 $\alpha$ ), rabbit polyclonal anti-p-PKR-like ER kinase (PERK), and rabbit polyclonal anti-X-box binding protein (XBP-1; all from Santa Cruz Biotechnology, Santa Cruz, CA); rabbit polyclonal anti-(active) Jun N-terminal kinase (JNK) and rabbit polyclonal anti-phospho-

p38 (Promega, Madison, WI); rabbit polyclonal anti-actin (Sigma, Taufkirchen, Germany); mouse monoclonal anti-ATF4 (Abnova GmbH, Heidelberg, Germany); mouse monoclonal anti-ATF6 $\alpha$  (Acris, Herford, Germany); rabbit polyclonal anti-LC3 (MBL, Nagoya, Japan); rabbit polyclonal anti-LMP7 (Novus Biologicals, Littleton, CO); rabbit polyclonal anti-PSMB5 (Abcam, Cambridge, UK); and mouse monoclonal anti-ubiquitin (Zymed Laboratories, Invitrogen Corporation, Carlsbad, CA). As secondary antibodies, we used HRP-conjugated goat anti-mouse immunoglobulin G (IgG), goat antirabbit IgG (Jackson ImmunoResearch Laboratories, Inc, West Grove, PA), and donkey anti-goat IgG (Santa Cruz Biotechnology). For flow cytometry, we used mouse anti-human CD243 (MDR1) AlexaFluor 647-conjugated antibody (Serotec, Düsseldorf, Germany). ELISA was performed with goat anti-human IgG (Jackson ImmunoResearch Laboratories, Inc) and HRP-conjugated goat anti-human IgG (Southern Biotech, Birmingham, AL).

### Reagents

Bortezomib (PS-341, Velcade; Janssen-Cilag, Neuss, Germany) and verapamil (Isoptin, Abbott) were obtained from the University Hospital Pharmacy, Erlangen. PS-1145 dihydrochloride (Sigma-Aldrich).

### Cell Lines and Culture Conditions

Cell lines used in this study were grown in RPMI 1640 medium supplemented with 50 U/ml penicillin, 50  $\mu$ g/ml streptomycin, 1 mM sodium pyruvate, 2 mM L-glutamine, 50  $\mu$ M  $\beta$ -mercaptoethanol, 10% fetal bovine serum for RPMI 8226 cells (myeloma), ARH 77 cells (plasma cell leukemia), and 20% bovine serum for JK-6L cells (myeloma) [9]. Cells were maintained at 37°C in a humidified incubator containing 5% CO<sub>2</sub>. The medium and all supplements were obtained from Gibco (Invitrogen, Karlsruhe, Germany).

### Viability Assay

Cells ( $1 \times 10^5$ ) were treated with 10 nM bortezomib and/or 70  $\mu$ M verapamil for 16 hours and incubated for another 4 hours with Alamar-Blue (BioSource International, Inc, Camarillo, CA). Activity of the mitochondrial dehydrogenase results in conversion of the coloring, which was followed by measurement of the absorption using a spectrophotometer (SpectraMax 190; Molecular Devices, Sunnyvale, CA).

### Flow Cytometric Analysis

Surface staining was performed as described [17]. The cells were analyzed by flow cytometry using a FACS Calibur (BD Biosciences, San Jose, CA). Data analyses were performed using the Cell Quest software (BD Biosciences).

### Cell Death Analysis

Cells ( $1 \times 10^5$ ) were treated with 10 nM bortezomib and/or 70  $\mu$ M verapamil for 16 hours. Fifty micromolars of the broad-range caspase inhibitor zVAD-FMK (Alexis Biochemicals, San Diego, CA) was used to block caspase activation. Staining with annexin V-fluorescein isothiocyanate (FITC; Genethor, Berlin, Germany) and propidium iodide (Sigma-Aldrich) was performed as described [18].

### Caspase 3/7 Assay

Cells ( $5 \times 10^4$ ) were treated with 10 nM bortezomib and/or 70  $\mu$ M verapamil for 16 hours. Caspase 3/7 activity was measured with the caspase-Glo-3/7 assay (Promega) according to the manufacturer's instructions. Luminescence was measured using the 96-well plate reader SpectraMax 190 (Molecular Devices, Sunnyvale, CA).

### Proteasomal Activity

Cells ( $2 \times 10^4$ ) were treated with 10 nM bortezomib and/or 70  $\mu$ M verapamil for 8 hours. The chymotrypsin-like activity was detected using the luminogenic proteasome substrate-based Proteasome-Glo Chymotrypsin-Like Cell-Based Assay Kit (Promega) according to the manufacturer's instructions. Luminescence was measured using the 96-well plate reader SpectraMax 190 (Molecular Devices, Sunnyvale, CA).

### Measurement of the Mitochondrial Potential

The fluorescent dye 3,3-dihexyloxycarbocyanine iodide (DiOC<sub>6</sub>; Sigma-Aldrich) was used to reveal disruption of the mitochondrial transmembrane potential ( $\Delta\Psi_m$ ). For measurement, cells ( $1 \times 10^5$ ) were treated with 40 nM bortezomib and/or 70  $\mu$ M verapamil for 10 hours. Afterward, cells were incubated with 120 nM DiOC<sub>6</sub> dye for 20 minutes at 37°C in the dark. Stained cells were resuspended in 20 ng/ml isotonic propidium iodide solution to exclude dead cells and were analyzed by flow cytometry (Epics XL; Coulter Co, Miami, FL).

### Reactive Oxygen Species Production

Cells ( $1 \times 10^5$ ) were treated with 40 nM bortezomib and/or 70  $\mu$ M verapamil and incubated for 2 hours with 10  $\mu$ M 2',7'-dichlorofluorescein diacetate (DCFH; Sigma-Aldrich) at 37°C. DCFH penetrates the cells and is in turn oxidized to DCF in the presence of reactive oxygen species (ROS). To eliminate ROS production, cells were preincubated with 10 mM *N*-acetylcysteine (NAC; Sigma-Aldrich) 1 hour before adding the inhibitors. H<sub>2</sub>O<sub>2</sub> (400  $\mu$ M) was selected as a donor to get maximal DCF intensity. DCF fluorescence intensity was determined by flow cytometric analysis (Epics XL; Coulter Co).

### Immunoblot Analysis

Cells ( $2 \times 10^6$ ) were treated with 10 nM bortezomib and/or 70  $\mu$ M verapamil for up to 16 hours. To generate total cell lysates, equal amounts of cells were washed with PBS and directly lysed in SDS sample buffer containing  $\beta$ -mercaptoethanol. For detergent-insoluble fractions, cells were lysed in TNES buffer (50 mM Tris-HCl, pH 7.5, 1% NP-40, 2 mM EDTA, 100 mM NaCl), with freshly added protease inhibitor cocktail (Serva, Heidelberg, Germany). The supernatants contain the soluble fractions. NP-40 detergent-insoluble pellets were resuspended in TNES buffer and sonicated for 10 seconds at 50 W on ice using a homogenizer (SONOPLUS; Bandlin Electronics, Berlin, Germany). Protein concentrations were colorimetrically determined using bicinchoninic acid (BCA Protein Assay; Pierce, Rockford, IL). Proteins were separated on 10% or 12% SDS-polyacrylamide gels and transferred onto nitrocellulose membranes (Schleicher & Schuell, Dassel, Germany). Membranes were blocked with 5% nonfat dry milk (Roth, Karlsruhe, Germany), probed with antibodies and developed using the enhanced chemiluminescence method.

### Electromobility Shift Analysis

Electromobility shift analysis (EMSA) was performed using oligonucleotides for NF- $\kappa$ B end labeled with IRDye according to the manufacturer's instructions (Metabion, Planegg-Martinsried, Germany). Briefly, cells ( $5 \times 10^6$ ) were treated with 10 nM bortezomib and/or 70  $\mu$ M verapamil for 8 hours, and nuclear extracts were prepared as previously described [9]. Ten microliters of probe mix (1  $\mu$ g poly-dIdC, 0.25% Tween 20, 0.1% NP-40, 20  $\mu$ g BSA, 1  $\times$  lipage buffer [0.1 M Tris-HCl, pH 7.5, 0.5 M NaCl, 10 mM EDTA, pH 7.5, 50% glycerol, before usage add 0.5 mM DTT], 0.1 pM oligo-IRDye-700) and

Orange G loading buffer (20 mg Orange G, 15% Ficoll) were added to 10  $\mu$ g of nuclear extracts. The reaction mixtures were incubated by gently shaking at room temperature for 30 minutes in the dark. After a prerun for 30 to 60 minutes at 150 V, samples were loaded on a 4% nondenaturing polyacrylamide gel and run for 2.5 hours at 150 V. Gels were analyzed using an Odyssey infrared imaging system (LI-COR Biosciences, Bad Homburg, Germany).

### Reverse Transcription-Polymerase Chain Reaction Analyses

Cells ( $2 \times 10^6$ ) were treated with 10 nM bortezomib and/or 70  $\mu$ M verapamil for up to 12 hours. Total RNA was isolated using the Mini RNAeasy Kit (Qiagen, Hilden, Germany), including digestion with RNase-free DNase. Complementary DNA (cDNA) synthesis from 1  $\mu$ g total RNA was performed using the SuperScript II Reverse Transcriptase (Invitrogen, Karlsruhe, Germany) and amplified with Taq polymerase (NEB, Frankfurt/Main, Germany) using specific primers for XBP-1. Polymerase chain reaction (PCR) products were separated by electrophoresis on 2% agarose gel and visualized by ethidium bromide staining. Levels of glyceraldehyde 3-phosphate dehydrogenase messenger RNA (mRNA) were used for adjustment of the mRNA concentrations. For quantitative real-time PCR analysis, the cDNA and appropriate primers were mixed with 2 $\times$  Absolute qRT-PCR SYBR green ROX reagent (Abgene, Hamburg, Germany). The following primers were used: CHOP forward, 5' GAAACGGAAACAGAGTGGTCA-TTCCCC 3', reverse, 5' GTGGGATTGAGGGTCACATCATTGG-CA 3'; mdr1 forward, 5' GCTCAGACAGGATGTGAGTTGG 3', reverse, 5' TAGCCCCCTTTAACTTGAGCAGC 3'. Primer sequences for I $\kappa$ B $\alpha$ , BiP, Bcl-2, Bax,  $\beta_5$ -subunit, and  $\beta$ -actin were retrieved from an online database (Primer Bank, Harvard.edu). Real-time PCR was performed in triplicates in an Applied Biosystems 7300 real-time PCR system (Applied Biosystems, Darmstadt, Germany).

### Enzyme-Linked Immunosorbent Assay

Sandwich ELISA was performed to quantify total IgG in the supernatant of JK-6L cells ( $2 \times 10^6$ ) treated with 10 nM bortezomib and/or 70  $\mu$ M verapamil for 16 hours. Diluted supernatants and standard sera (Jackson ImmunoResearch Laboratories, Inc) were incubated on IgG-coated Maxisorp microplates (Thermo Fisher Scientific, Roskilde, Denmark), and bound IgG was detected with horseradish peroxidase-conjugated IgG. *O*-phenylenediamine dihydrochloride (Sigma-Aldrich) was used as substrate. Optical density was measured at 495 nm in a SpectraMax 190 ELISA reader (Molecular Devices, Ismaning, Germany).

### Transmission Electron Microscopy

Cells ( $2 \times 10^6$ ) treated with bortezomib and/or verapamil were fixed in 2.5% glutaraldehyde in 0.2 M phosphate buffer (pH 7.4), postfixed in 2% buffered osmium tetroxide, dehydrated in graded alcohol concentrations, and embedded in epoxy resin according to standard protocols. For orientation, 1- $\mu$ m semithin sections were stained with toluidine blue. Ultrathin sections were stained with uranyl acetate and lead citrate and examined using a transmission electron microscope (EM 906E; Carl Zeiss NTS GmbH, Oberkochen, Germany).

## Results

### Verapamil Synergistically Decreased Viability of Bortezomib-Treated Myeloma Cell Lines

We first assessed the effect of bortezomib and verapamil alone and in combination on the viability of myeloma cell lines. The concentrations

necessary for efficient depletion of myeloma cells were determined by performing titration curves. On the basis of this titration, we used 70  $\mu$ M verapamil and a minimum of 10 nM bortezomib in the following studies (Figure 1A). Importantly, the combination of bortezomib and verapamil markedly declined the viability of the JK-6L, RPMI 8226, and ARH-77 cell lines after 16 hours of culture (Figure 1B). Bortezomib reduced the viability of all used myeloma cell lines, whereas verapamil alone exhibited just a slight cytotoxic effect on JK-6L cells but none on RPMI 8226 and ARH-77 cells. Compared with the other cell lines, JK-6L cells were more sensitive toward bortezomib and verapamil treatment, most likely because of their higher immunoglobulin chain expression as analyzed by intracellular flow cytometry and secretion assays (data not shown), consistent with previous results [9,10]. Most of the following analyses were performed with the JK-6L cell line because it is especially sensitive against bortezomib and verapamil.

Next we analyzed the induction of cell death on bortezomib and verapamil treatment. As displayed in Figure 1C, the combination of bortezomib and verapamil markedly diminished the percentage of annexin V/propidium iodide double-negative viable myeloma cells while increasing apoptosis and necrosis, especially in JK-6L cells. At earlier time

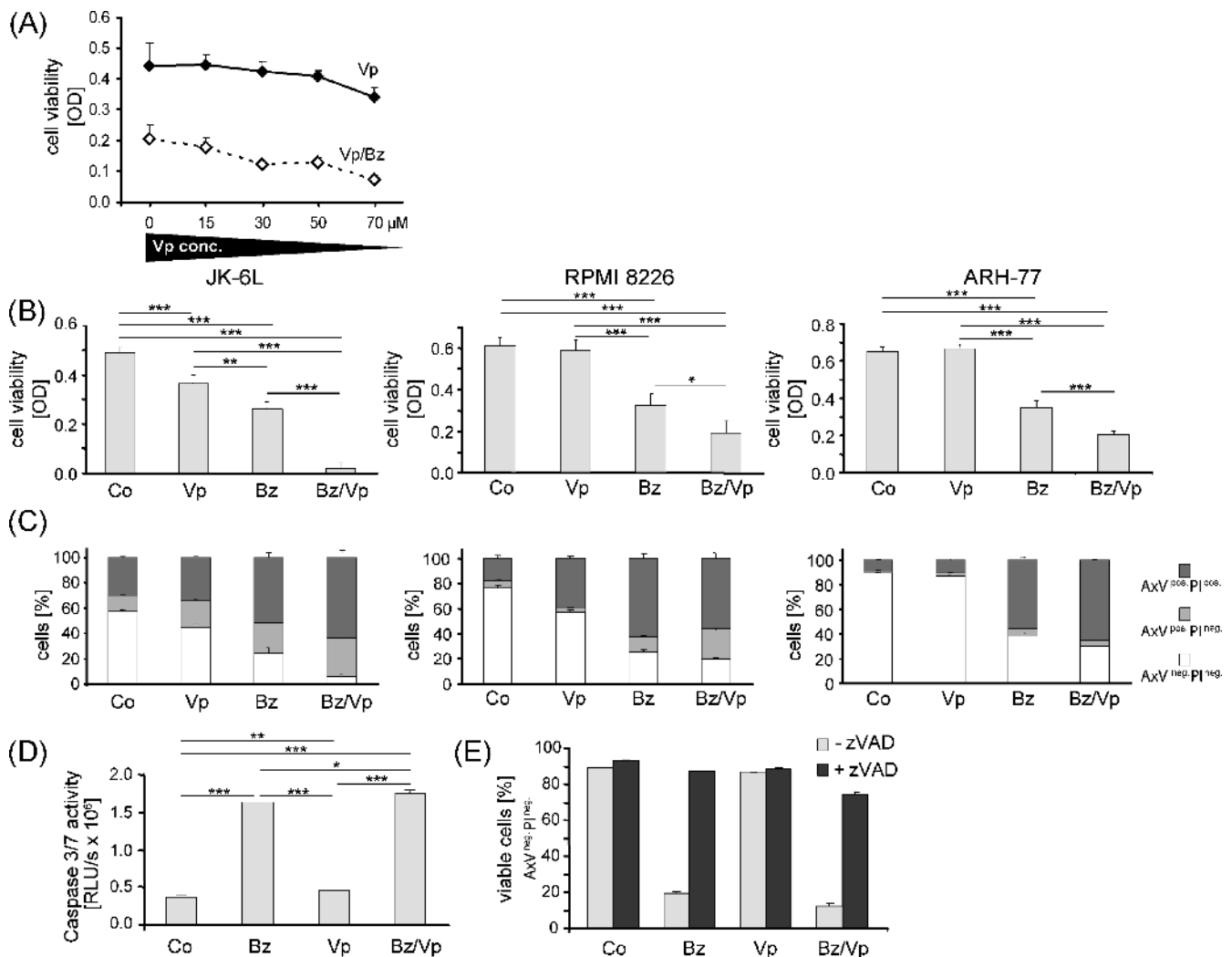


**Figure 1.** Bortezomib together with verapamil synergistically reduces viability in human myeloma cell lines. (A) JK-6L cells were treated with increasing concentrations of verapamil as indicated (solid line) and in combination with 10 nM bortezomib (discontinuous line) for 16 hours. Cells were incubated with the vital dye AlamarBlue. The absorbance (OD) was measured using a spectrophotometer. Mean values and SD were calculated from triplicates. (B) Myeloma cell lines were treated with 10 nM bortezomib and 70  $\mu$ M verapamil or the combination of both inhibitors for 16 hours. Cells were incubated with the vital dye AlamarBlue. The absorbance (OD) was measured using a spectrophotometer. Mean values and SD were calculated from hexaplicates. (C) Myeloma cell lines were treated with 10 nM bortezomib and 70  $\mu$ M verapamil or the combination of both inhibitors for 16 hours. Diagrams show the percentages of viable (annexin V-FITC<sup>negative</sup>/propidium iodide<sup>negative</sup>), apoptotic (annexin V-FITC<sup>positive</sup>/propidium iodide<sup>negative</sup>), and necrotic/late apoptotic (annexin V-FITC<sup>positive</sup>/propidium iodide<sup>positive</sup>) cells, analyzed by flow cytometry. Mean values and SD were calculated from triplicates. (D) JK-6L cells were treated with 10 nM bortezomib and 70  $\mu$ M verapamil or the combination of both inhibitors for 16 hours. Caspase 3/7 activity was determined using the luminescence-based Caspase-Glo assay. Mean values and SD were calculated from quadruplicates. (E) JK-6L cells were treated with the inhibitors in the presence or absence of the caspase inhibitor zVAD-FMK. The diagrams show the percentages of viable cells (annexin V-FITC<sup>negative</sup>/propidium iodide<sup>negative</sup>) analyzed by flow cytometry. Mean values and SD were calculated from triplicates. All these data represent one of three independently done experiments. Student's *t*-test for unpaired heteroscedastic samples was used for statistical analysis. #*P* < .05, \**P* < .01, \*\**P* < .001, \*\*\**P* < .0001. AxV indicates annexin V-FITC; Bz, bortezomib; Co, control (PBS-treated); PI, propidium iodide; Vp, verapamil.

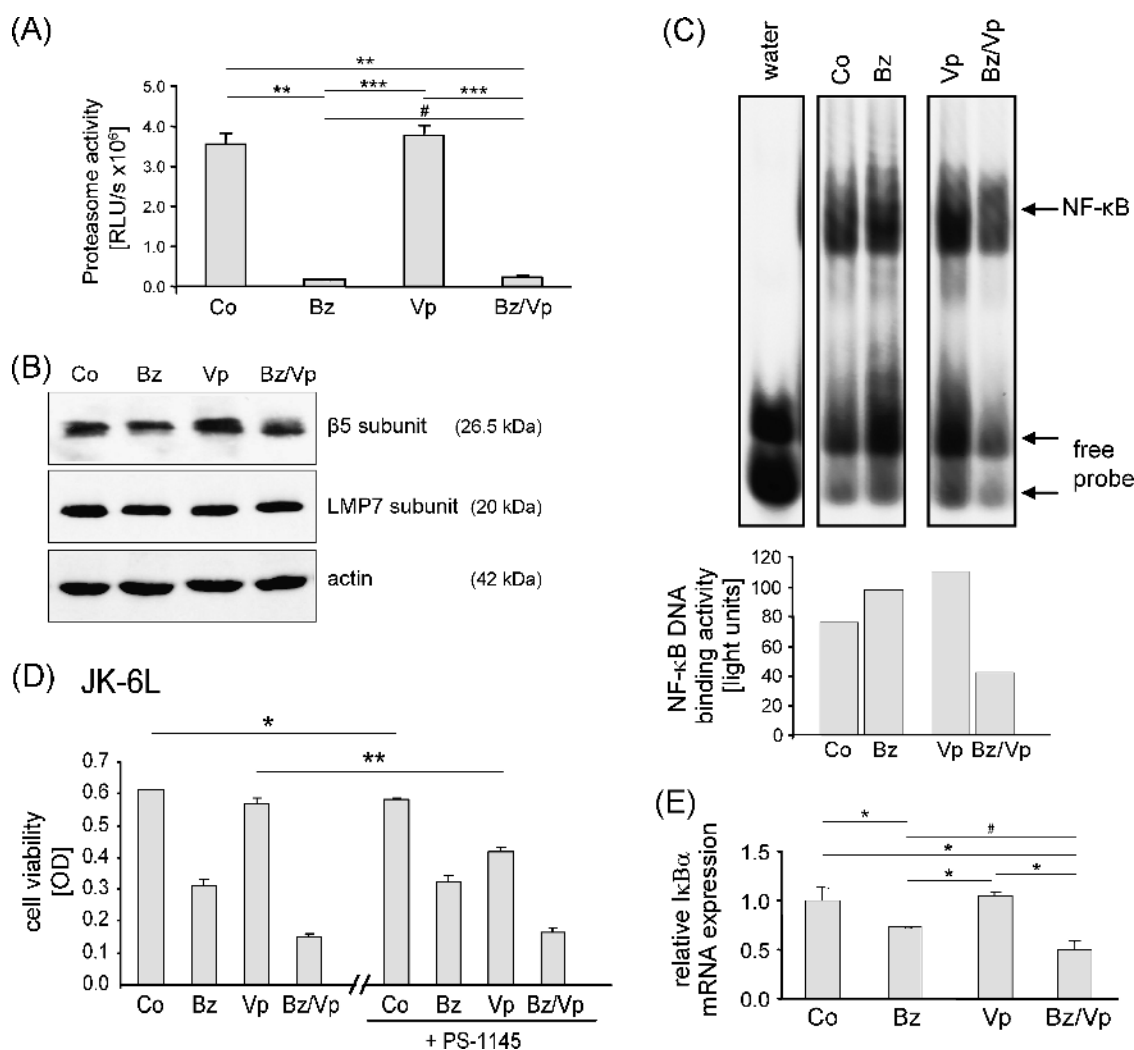


**Figure 2.** JK-6L cells show decreased NF-κB activity on bortezomib and verapamil combination. (A) Proteasomal activity of JK-6L cells treated with 10 nM bortezomib and/or 70 μM verapamil for 8 hours. The chymotrypsin-like activity was determined using the luminescence-based Proteasome-Glo assay. Mean values and SD were calculated from quadruplicates. Data represent one of three independently experiments. (B) Western blot analysis of total cell lysates from JK-6L cells treated with 10 nM bortezomib and/or 70 μM verapamil for 8 hours. Anti-actin antibody staining served as control for an equal loading. One representative immunoblot of two independent experiments is shown. (C) EMSA was performed with nuclear extracts prepared from JK-6L cells treated with 10 nM bortezomib and/or 70 μM verapamil for 8 hours. NF-κB DNA-binding activity was analyzed using IRDye end-labeled probes containing specific binding sites. As control, gel was loaded with free-labeled probes without nuclear extract. The intensity of NF-κB DNA binding activity is displayed as arbitrary light units. Data represent one of two independently performed experiments. (D) Myeloma cell lines were treated with 10 nM bortezomib and 70 μM verapamil or the combination of both inhibitors in the absence or presence of 20 μM NF-κB inhibitor PS-1145 for 16 hours. Cells were incubated with the vital dye AlamarBlue. The absorbance (OD) was measured using a spectrophotometer. Only relevant significance values were depicted. (E) Quantitative real-time PCR analysis of total RNA isolated from JK-6L treated with 10 nM bortezomib and/or 70 μM for 8 hours. The diagrams show the relative IκBα mRNA levels of bortezomib-treated JK-6L cells normalized to β-actin mRNA levels, which served as internal control. cDNA from PBS-treated cells served as reference control. The comparative Ct (DDCT) method for relative quantification of gene expression was used. Mean values and SD were calculated from triplicates. Data represent one of two independently done experiments. Student's *t*-test for unpaired heteroscedastic samples was used for statistical analysis. #*P* < .05, \**P* < .01, \*\**P* < .001, \*\*\**P* < .0001. *Bz* indicates bortezomib; *Co*, control (PBS-treated); *Vp*, verapamil.

points, we could detect almost exclusively apoptotic cells and not necrotic ones (data not shown). Hence, combination of bortezomib and verapamil may induce predominantly apoptotic cell death, and the annexin V/propidium iodide-positive cells represent late apoptotic rather than primary necrotic cells. In contrast to verapamil alone, bortezomib, and even more when combined with verapamil, strongly induced activation of caspase 3/7 (Figure 1D). To evaluate the functional importance of bortezomib- and verapamil-induced caspase activation for apoptosis, we examined the influence of the pan-caspase inhibitor zVAD-FMK.

Figure 1E shows that zVAD-FMK significantly interfered with cell death triggered either by the combination of both inhibitors or by bortezomib alone. Thus, bortezomib-induced apoptotic cell death was significantly enhanced in the presence of verapamil.

#### Proteasomal Activity Was Not Altered by Verapamil

To elucidate the mechanisms by which verapamil enhances the anti-myeloma effect of bortezomib, we first analyzed the proteasomal activity of the JK-6L cells during the treatment. The chymotrypsin-like activity

of the 20S proteasome was completely blocked by bortezomib, whereas it was not affected by verapamil alone. Also, the combination of bortezomib and verapamil did not further decrease the proteasomal activity (Figure 2A). The concentration of the subunit  $\beta_5$  accounting for the chymotrypsin-like activity of the constitutive 26S proteasome moderately decreased after incubating with bortezomib (Figure 2B). Beside that, the immunoproteasomal subunit LMP7 that corresponds to  $\beta_5$  was not altered after treatment with the inhibitors (Figure 2B). Verapamil itself exerts no major effect on proteasomal activity.

### *Combination of Verapamil and Bortezomib Resulted in NF- $\kappa$ B Inhibition*

The transcription factor NF- $\kappa$ B was shown to be constitutively active in myeloma cells and to be essential for their survival [19]. To quantify the NF- $\kappa$ B DNA-binding activity, nuclear extracts from JK-6L cells treated with bortezomib and/or verapamil were analyzed by EMSA (Figure 2C). Bortezomib together with verapamil markedly decreased the NF- $\kappa$ B DNA-binding activity in JK-6L myeloma cells, whereas bortezomib or verapamil alone rather somewhat increased the constitutive NF- $\kappa$ B activity after 8 hours (Figure 2C). Incubation of JK-6L cells with an IKK inhibitor combined with verapamil resulted in a stronger reduction of the cell viability than in cells treated with verapamil only, suggesting that this specific NF- $\kappa$ B blockade may account for verapamil-induced synergistic cytotoxicity (Figure 2D).

We also measured the I $\kappa$ B $\alpha$  mRNA expression, which is strongly induced by NF- $\kappa$ B activation and therefore reflects transcriptional activity of NF- $\kappa$ B [20]. Consistent with NF- $\kappa$ B DNA-binding activity, the relative I $\kappa$ B $\alpha$  mRNA concentrations dropped on the combination treatment (Figure 2D), indicating that NF- $\kappa$ B transcriptional activity was decreased. Thus, the blockade of the survival factor NF- $\kappa$ B on combination of bortezomib with verapamil might be crucial for enhancement of cell death.

### *Verapamil Enhanced Bortezomib-Triggered UPR Signals*

To investigate whether verapamil together with bortezomib induced terminal UPR signals, we analyzed prominent UPR components in lysates of JK-6L cells. Enhanced chaperone production is a hallmark of UPR activation. Induction of the ER resident chaperone  $\mu$ -heavy chain binding protein (BiP) is observed in bortezomib-treated cells. However, there was no additional increase of BiP expression in the presence of verapamil (Figure 3A). GRP94 was slightly upregulated on combination therapy compared with monotherapy. Hsp70, however, was strongly induced by bortezomib and its expression was further augmented in combination with verapamil (Figure 3A).

The transmembrane factor ATF6 induces transcription of several genes including chaperones, XBP-1, and CEB/P homologous protein (CHOP) in response to ER stress [21]. After bortezomib and/or verapamil treatment, ATF6 was activated as shown by reduced expression of its inactive 90-kDa precursor form (Figure 3A). We also observed a slight induction of XBP-1 mainly triggered by bortezomib. The spliced XBP-1 protein was present in bortezomib-treated cells and synergistically increased on bortezomib and verapamil application (Figure 3A). Splicing of XBP-1 mRNA is induced by IRE1 $\alpha$  to generate a transcript encoding an XBP-1 protein. The splicing results in the translation of a larger XBP-1 protein [22]. In contrast to protein expression, analysis of XBP-1 mRNA revealed a strong activation of XBP-1 evidenced by the generation of the two splicing products on treatment with bortezomib plus verapamil (Figure 3B). The proapoptotic factor CHOP is

markedly induced in cells incubated with bortezomib plus verapamil (Figure 3A), suggesting that verapamil strengthened the effect of the proteasome inhibitor.

As shown in Figure 3A, IRE1 expression itself was upregulated after bortezomib/verapamil treatment compared with monotherapy, indicating that verapamil enhanced the effect of bortezomib. On ER stress, IRE1 stimulates p38, causing activation of JNK. The p38 mitogen-activated protein kinase was highly activated evidenced by a strong expression of phosphorylated p38 (Figure 3A). Bortezomib/verapamil treatment eventually induced active JNK2 proposed to promote cell death (Figure 3A). These results imply that the ATF6/IRE1 signaling plays an important role in the bortezomib/verapamil-mediated ER stress response.

In cells with irrecoverable levels of ER stress, the IRE1 pathway can promote apoptosis by interaction with Bcl-2 family members [23]. The proapoptotic factor Bax is strongly expressed in double-treated JK-6L cells, whereas Bcl-2 was not markedly altered, if at all there was a slight increase on treatment with either bortezomib or verapamil alone (Figure 3A). The BH3-only protein Bim, a crucial effector of the IRE1-JNK pathway [24], was also induced by bortezomib together with verapamil. Induction of the key UPR molecules BiP, CHOP, Bim, and Bax could be confirmed in the myeloma cell lines ARH-77 and RPMI 8226 (Figure 3A).

PERK phosphorylates and inactivates the eukaryotic elongation factor eIF2 $\alpha$  reducing the protein load through translational attenuation. Active p-eIF2 $\alpha$  increases expression of the transcription factor ATF4, which induces UPR target genes [21]. Western blot analyses revealed increasing PERK phosphorylation in bortezomib-, verapamil-, and bortezomib/verapamil-treated cells (Figure 3A). We also detected highly activated eIF2 $\alpha$  in samples incubated with bortezomib plus verapamil (Figure 3A). At early time points, ATF4 was only induced in cells treated with verapamil after 16 hours; however, ATF4 expression was augmented on all different treatment regimens (Figure 3A). These data suggest a possible role for the PERK pathway in bortezomib/verapamil-mediated cellular effects, most notably for the calcium channel blocker verapamil.

To confirm induction of the UPR target genes on the transcriptional level, we performed quantitative reverse transcription-PCR. Here, we focused on UPR genes that are mainly involved in mediating survival and apoptosis. In contrast to BiP protein synthesis, we observed a stronger increase of BiP mRNA in cells treated with the drug combination (Figure 3C). Consistent with protein expression, analysis of CHOP mRNA revealed a more than 40-fold higher expression in response to bortezomib plus verapamil compared with untreated cells (Figure 3C). Bcl-2 mRNA was slightly downregulated, whereas Bax was increased by adding bortezomib plus verapamil (Figure 3C). Hence, bortezomib-triggered transcriptional activation of the terminal UPR was enhanced by combination with verapamil.

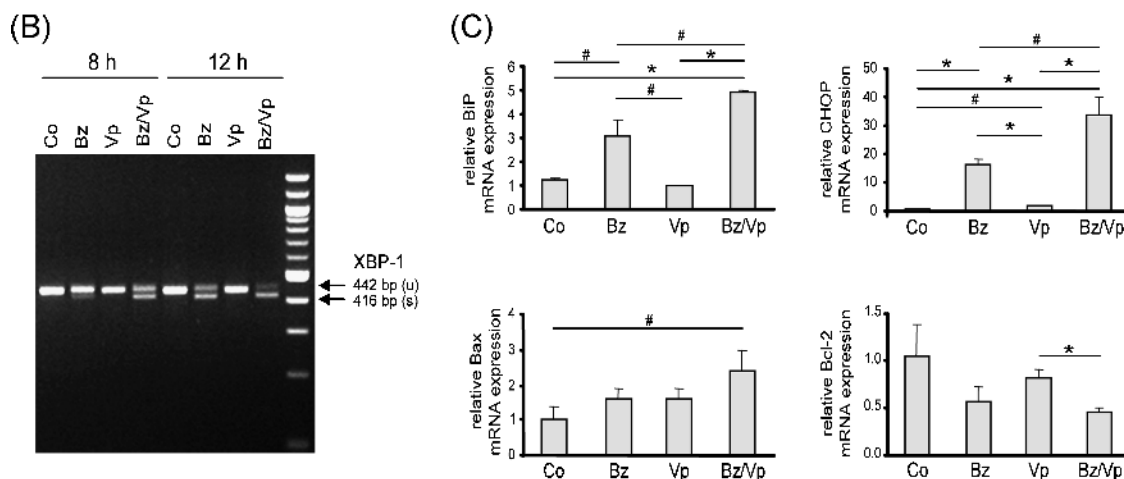
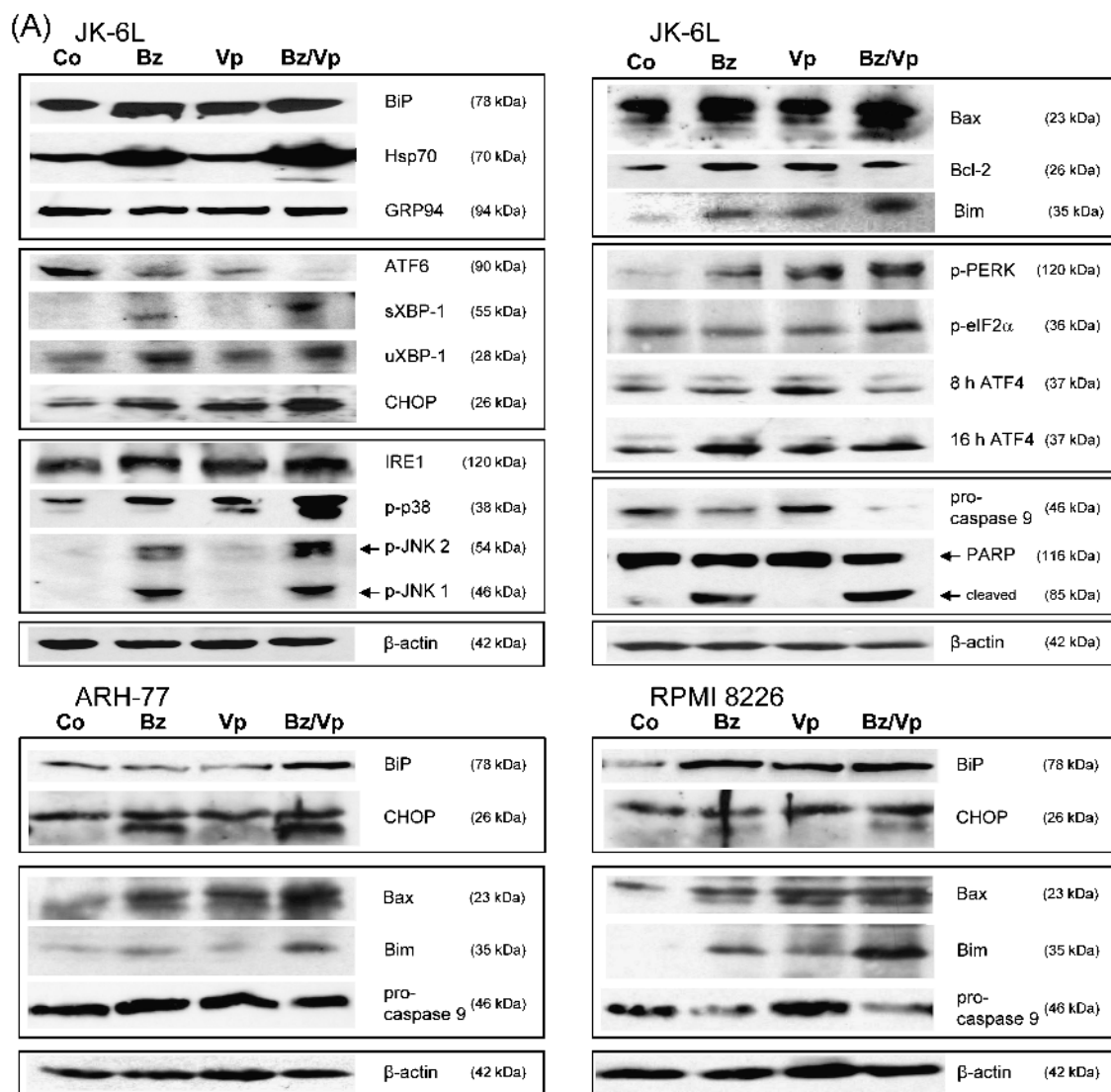
### *Bortezomib Plus Verapamil Activated Caspases*

JNK activation can promote apoptosis in cells with overwhelming stress through activation of caspases [25]. Hence, we investigated whether the inhibitors bortezomib and verapamil lead to caspase activation. Figure 3A demonstrates that after treatment with the drug combination, procaspase 9 virtually disappeared, indicating caspase 9 activation; verapamil alone had no effect on caspase 9 activation. Activation of the procaspase 9 was also observed in the ARH-77 and RPMI 8226 myeloma cell lines (Figure 3A). Likewise, a luminescence-based assay revealed that caspase 3/7 activation is more pronounced on the

combination of bortezomib and verapamil than after monotherapy (Figure 1D). Further, bortezomib induced PARP activation as evidenced by detection of the cleavage product. The cleavage band was induced by bortezomib and even stronger in combination with verapamil (Figure 3A). Together, the bortezomib plus verapamil treatment resulted in caspase activation followed by PARP cleavage, finally leading to cell death.

*Accumulation of Polyubiquitinated Proteins in Cells Incubated with Verapamil/Bortezomib*

To be degraded by the 26S proteasome, misfolded proteins have to get ubiquitinated. On proteasome inhibition, these proteins can accumulate as insoluble intracellular aggregates up to cytotoxic levels [26]. As depicted in Figure 4A, both bortezomib and verapamil induced



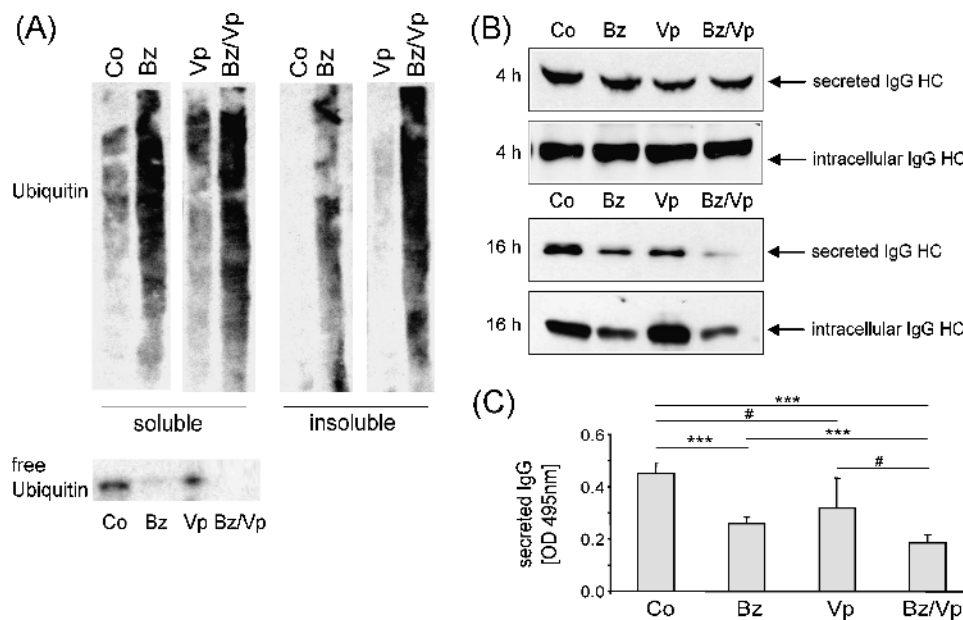


**Figure 4.** JK-6L cells show enhanced protein accumulation in the presence of bortezomib and verapamil. (A) Western blot analysis of detergent-soluble and detergent-insoluble fractions of JK-6L cells treated with 10 nM bortezomib and/or 70 μM verapamil for 16 hours. Immunoblot analysis was done using an anti-ubiquitin antibody. To detect free ubiquitin, a denser gel was used. One representative immunoblot of two independent experiments is shown. (B) Western blot analysis of total cell lysates from JK-6L cells treated with 10 nM bortezomib and/or 70 μM verapamil for 16 hours. Immunoblot analysis was done using HRP-conjugated anti-IgG antibody. One representative immunoblot of two independent experiments is shown. (C) IgG concentration in the supernatant of JK-6L cells treated with 10 nM bortezomib and/or 70 μM verapamil for 16 hours was determined by ELISA. The absorbance (OD) was measured using a spectrophotometer. Mean values and SD were calculated from hexaplicates. Data represent one of two independently done experiments. Student's *t*-test for unpaired heteroscedastic samples was used for statistical analysis. #*P* < .05, \**P* < .01, \*\**P* < .001, \*\*\**P* < .0001. Bz indicates bortezomib; Co, control (PBS-treated); HC, heavy chain; Vp, verapamil.

accumulation of ubiquitinated proteins after 16 hours in the soluble and insoluble fractions; also, after 8 hours, we observed ubiquitinylation of soluble but not of insoluble proteins (Figure W1). There was no marked further increase of ubiquitinated proteins in the soluble fractions after combination treatment, also reflected by the pool of free ubiquitin. However, the amount of ubiquitinated proteins in detergent-insoluble fractions was much higher in the presence of bortezomib plus verapamil, indicating an increased formation of intracellular protein aggregates.

Further, verapamil as well as bortezomib leads to the reduction of IgG in the supernatant of JK-6L cells as observed by ELISA and Western blot analysis. Intracellular IgG was upregulated by adding verapamil (Figure 4B). Hence, bortezomib reduced IgG secretion presumably by UPR-mediated blockade of protein synthesis; whereas verapamil may

interfere with IgG secretion (Figure 4C). We exclude the induction of apoptosis because IgG expression was also reduced at earlier time points (4 hours; Figure 4B).

#### *Vast Dilation of the ER and Induction of an Autophagy-like Process on Combination Therapy*

To assess subcellular alterations induced by bortezomib and verapamil, we performed transmission electron microscopy of JK-6L cells. Bortezomib treatment resulted in ER dilation after 8 hours, most likely induced through accumulation of misfolded proteins, which even further increased after 16 hours (Figure 5A). Importantly, we observed vesicle-like intracellular structures after verapamil administration, suggesting that calcium channel blockade induced autophagy in the myeloma cells (Figure 5A). Visible signs of ER stress evidenced by ER

**Figure 3.** Verapamil enhances the bortezomib-induced UPR activation in JK-6L cells. (A) Western blot analysis of total cell lysates from JK-6L, ARH-77, and RPMI 8226 cells treated with 10 nM bortezomib and/or 70 μM verapamil for 16 hours. Anti-actin antibody staining served as control for equal loading. One representative immunoblot of three independent experiments is shown. (B) Reverse transcription-PCR analysis of total RNA isolated from JK-6L cells treated with 10 nM bortezomib and/or 70 μM verapamil. Reverse transcription-PCR was done using a primer set that detects the unspliced (442 bp) and spliced (416 bp) form of XBP-1 mRNA. Data represent one of two independently done experiments. (C) Quantitative real-time PCR analysis of total RNA isolated from JK-6L cells treated with 10 nM bortezomib and/or 70 μM verapamil for 12 hours. The diagrams show relative mRNA levels of treated JK-6L cells normalized to β-actin mRNA levels, which served as internal control. cDNA from PBS-treated cells served as reference control. The comparative Ct (DDCT) method for relative quantification of gene expression was used. Mean values and SD were calculated from triplicates. Data represent one of two independently done experiments. Student's *t*-test for unpaired heteroscedastic samples was used for statistical analysis. #*P* < .05, \**P* < .01, \*\**P* < .001, \*\*\**P* < .0001. Bz indicates bortezomib; Co, control (PBS-treated); Vp, verapamil; XBP-1u, unspliced; XBP-1s, spliced.

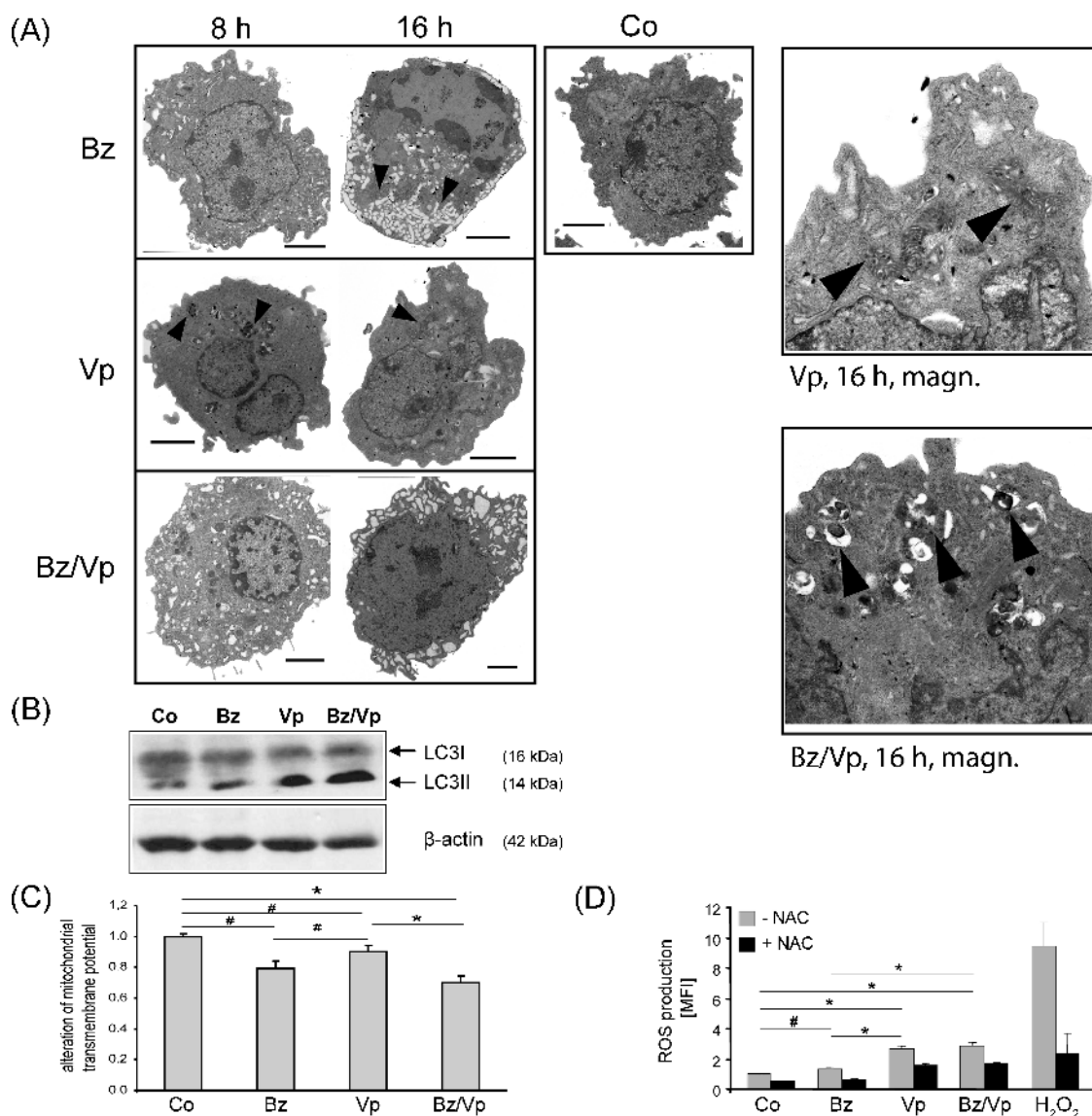


**Figure 5.** Verapamil induces an autophagy-like process in JK-6L cells. (A) Transmission electron microscopy analysis of ultrathin sections of JK-6L cells treated with 10 nM bortezomib and/or 70  $\mu$ M verapamil for 16 hours. Bortezomib-treated cells show dilated ER (arrows). Verapamil-treated cells contain autophagosomes (arrows) and expanded mitochondria (one arrow). The magnification of verapamil-treated cells displays in greater detail the expanded and stressed mitochondria (upper right panel). The lower right panel shows a magnification of cells treated with bortezomib and verapamil, clearly displaying autophagosomes engulfing cellular constituents. The scale bar shows a longitude of 2.0  $\mu$ m. (B) Western blot analysis of total cell lysates from JK-6L cells treated with 10 nM bortezomib and/or 70  $\mu$ M verapamil for 16 hours. Cell lysates were separated by SDS-PAGE on a 12% polyacrylamide gel, and immunoblot analysis was done using an anti-LC3 antibody. Antiactin antibody staining served as control for equal loading. (C) Mitochondrial transmembrane potential of JK-6L cells treated with 40 nM bortezomib and/or 70  $\mu$ M verapamil for 10 hours. Cells were double stained with DiOC<sub>6</sub> dye and propidium iodide (to exclude necrotic cells) and analyzed by flow cytometry. The alteration of the mitochondrial transmembrane potential of propidium iodide<sup>negative</sup>/DiOC<sub>6</sub><sup>positive</sup> cells is displayed in the diagram. The control was set as 1.0. Mean values and SD were calculated from triplicates. Data represent one of two independently performed experiments. (D) ROS production of JK-6L cells treated with 40 nM bortezomib and/or 70  $\mu$ M verapamil for 2 hours and incubated in the presence of with DCFH. The DCF fluorescence intensity was determined by flow cytometric analysis. H<sub>2</sub>O<sub>2</sub> served as positive control. To eliminate ROS production, cells were treated with NAC. The mean fluorescence intensities (MFI) are displayed in the diagram. Mean values and SD were calculated from triplicates. Data represent one of three independently performed experiments. Student's *t*-test for unpaired heteroscedastic samples was used for statistical analysis. #*P* < .05, \**P* < .01, \*\**P* < .001, \*\*\**P* < .0001. Bz indicates bortezomib; Co, control (PBS-treated); Vp, verapamil.

expansion together with the appearance of protein deposits were detected 8 hours after combined treatment with bortezomib plus verapamil (Figure 5A). Aside increased autophagosomes, a vast swelling of the mitochondria was also observed after incubation with verapamil (Figure 5A). Consistent with the viability and UPR data, we observed

a massive ER expansion along with vacuolization accompanied by morphologic features of apoptosis after 16 hours of incubation with this drug combination (Figure 5A).

To corroborate the morphologic evidence of verapamil-induced autophagy in myeloma cells, we analyzed the autophagosome formation

using the microtubule-associated protein 1 light chain 3 (LC3; Figure 5B). LC3 is processed posttranslationally into LC3-I, then converted to LC3-II that is specifically associated with autophagosome membranes [27]. LC3-II concentrations, correlating with autophagosome numbers, were increased by verapamil and even further in combination with bortezomib, suggesting enhanced autophagy (Figure 5B).

Changes in mitochondrial structure may correlate with dysfunction of the mitochondria. We therefore determined the mitochondrial membrane potential: The percentage of DiOC<sub>6</sub>-positive cells decreased in the presence of the drugs (Figure 5C), indicating that both bortezomib and verapamil induced disruption of the mitochondrial membrane potential. However, the loss of the mitochondrial potential was more pronounced in bortezomib-treated than in verapamil-treated cells.

Importantly, in response to verapamil treatment, we observed a vast and significant accumulation of ROS, which was reduced by the antioxidant NAC (Figure 5D), possibly linking increased ROS production to depolarization of the inner mitochondrial membrane.

### Verapamil Decreased P-gp Expression in Myeloma Cells

As verapamil diminished expression of P-gp in resistant leukemic cells [16], we determined the effect of verapamil and bortezomib on P-gp expression on JK-6L cells. Flow cytometric analyses revealed decreased expression of P-gp on the JK-6L cells when treated with verapamil (Figure 6A). There was a slight effect of bortezomib alone but no synergistic effect together with verapamil on P-gp expression (Figure 6A). MDR1

mRNA levels significantly declined on verapamil monotherapy (Figure 6B). Hence, we conclude that P-gp expression on JK-6L was predominantly inhibited by verapamil.

### Discussion

Bortezomib exhibits antitumor activities by inducing cell death, but long-term administration often leads to secondary resistance of myeloma cells [19]. To overcome cellular resistance and to enhance bortezomib's selectivity for myeloma cells, we searched for agents that synergistically increase the antitumor effect of bortezomib. The calcium channel blocker verapamil represented a promising candidate because it was shown to reduce MDR1-mediated drug resistance in leukemia cells [16]. Our present study revealed that verapamil enhanced the anti-myeloma effect of bortezomib leading to increased cell death in myeloma cells. It remains to be investigated if such high plasma levels of verapamil required to exert synergistic effects can be achieved *in vivo* without serious toxicity. ROS production and autophagy-like processes induced by verapamil might contribute to elevation of proapoptotic stress signals, strongly activating the terminal UPR in bortezomib-treated cells.

One important mechanism of bortezomib is the UPR induction that can trigger tumor cell death due to prolonged ER stress. This stress response can be induced through accumulation of misfolded immunoglobulin chains/DRiPs in the ER caused by proteasome inhibition [9,28]. Our results demonstrated that verapamil is able to enhance proapoptotic stress signals triggered by bortezomib. Depending on the UPR branch, the calcium channel inhibitor verapamil alone had only slight effects on UPR induction compared with bortezomib or the combination therapy. Also, verapamil displayed no direct effect on the 26S proteasome activity, suggesting that the ER-associated degradation is not blocked by verapamil. In contrast to our findings, Fekete et al. [29] observed an inhibition of proteasomal activity by verapamil in human epitheloid carcinoma cells; possibly, this discrepancy is due to the different reactions of individual cell species.

The expression of the chaperone BiP did not markedly change between treated cells, likely because of the relatively high basal levels of this protein often found in myeloma cells [10]; the BiP mRNA, however, was strongly induced. Likewise, an increase in cellular BiP mRNA does not necessarily lead to increased synthesis of BiP, and protein levels can remain constant [30]. A need for more folding capacity was also evidenced by an induction of the ER resident chaperone GRP94 after bortezomib/verapamil treatment. Hsp70, the cytosolic homolog of BiP, was markedly increased in the presence of bortezomib and verapamil, indicating activation of a mitochondrial-like stress [31]. One function of chaperones is to protect cells against ER stress-induced apoptosis, but in case of prolonged or overwhelming stress signals, the UPR ends in apoptosis. In our approach, the IRE1-mediated pathway was profoundly activated. By recruiting TRAF2, IRE1 leads to increased levels of phosphorylated p38 mitogen-activated protein kinase causing JNK activation [32] that can foster apoptosis through activation of caspases under severe stress induction [25]. On treatment with the combination of bortezomib and verapamil, p38 was strongly activated followed by JNK activation, suggesting that the IRE1-p38-JNK signaling plays an important role in bortezomib/verapamil-mediated cell death.

Also, CHOP expression is enhanced by verapamil when combined with bortezomib. CHOP, which is associated with the terminal UPR and apoptosis, was shown to downregulate Bcl-2 [33]. A recent publication demonstrated that CHOP itself is not essential for physiologic cell death in mouse B and plasma cells [34]. Expression of the proapoptotic Bax increased in response to combination treatment, whereas there

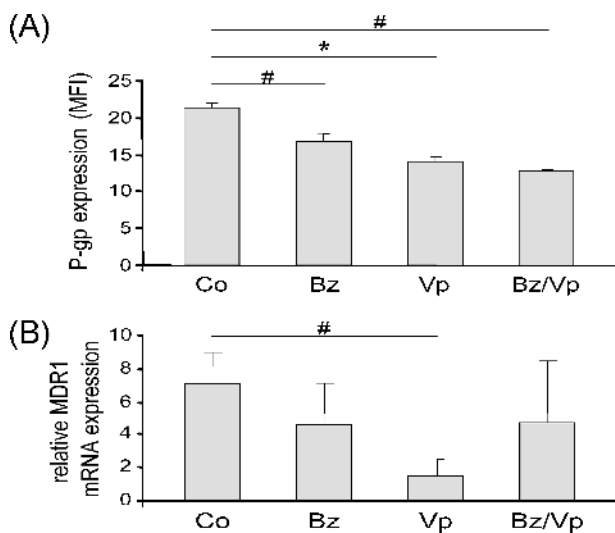


**Figure 6.** Verapamil impairs P-gp function in JK-6L cells. (A) Quantitative real-time PCR analysis of total RNA isolated from JK-6L cells treated with 10 nM bortezomib and/or 70  $\mu$ M verapamil for 12 hours. The diagram shows relative MDR1 mRNA levels of treated JK-6L cells normalized to  $\beta$ -actin mRNA levels, which served as internal control. cDNA from PBS-treated cells served as reference control. The comparative Ct (DDCT) method for relative quantification of gene expression was used. (B) Surface expression of MDR1 on JK-6L cells treated with 10 nM bortezomib and/or 70  $\mu$ M verapamil for 16 hours was analyzed by flow cytometry. Mean values and SD were calculated from triplicates. All these data represent one of two independently performed experiments. Student's *t*-test for unpaired heteroscedastic samples was used for statistical analysis. #*P* < .05, \**P* < .01, \*\**P* < .001, \*\*\**P* < .0001. Bz indicates bortezomib; Co, control (PBS-treated); Vp, verapamil.

was no significant difference in Bcl-2 levels. Importantly, Bax and Bcl-2 can also activate IRE1 [23], thereby providing a connection between UPR and apoptosis pathways. The role of CHOP in human myeloma cells is not yet resolved.

The role of the PERK pathway in cell death regulation remains to be elucidated. Its activation initiates inhibition of translation via phosphorylation of eIF2 $\alpha$  to protect the cell from protein overload. The PERK pathway was highly activated on treatment with verapamil and the combination of bortezomib and verapamil as shown by up-regulation of p-eIF2 $\alpha$ , suggesting attenuation of mRNA translation. In addition, PERK-mediated eIF2 $\alpha$  phosphorylation contributes to transcriptional activation of ATF4, which has been shown to stimulate expression of autophagy genes [35] and to induce CHOP [21]. Also, long-lasting suppression of protein synthesis is not compatible with cell survival and can induce autophagy known to require PERK and eIF2 $\alpha$  phosphorylation. Using transmission electron microscopy, we detected a vast expansion of mitochondria and formation of cytosolic vesicles on verapamil exposure. These observations suggest that verapamil induces autophagy in the myeloma cells. Autophagy, an intracellular degradation system of cytoplasmic contents and organelles, is required for normal turnover of cellular components during starvation in eukaryotic cells. The autophagosomes, with two or more membranes enclosed vesicles, engulf various cellular constituents that fuse with lysosomes for degradation and recycling [36]. Autophagy is also characterized by dilation of mitochondria that we observed in treated JK-6L cells. Besides promoting cell survival, autophagy can trigger caspase-independent cell death [36]. Likewise, we observed no caspase activation by verapamil. A very recent study by Williams et al. [37] revealed that verapamil stimulates autophagy by reducing the calcium influx. Notably, verapamil diminished the intracellular calcium level also in the myeloma cell lines (Figure W2). Changes in calcium homeostasis may foster ER stress triggering autophagy by the ER-activated autophagy pathway. The latter could be mediated by limited UPR signals involving PERK and/or IRE1 as well as UPR-independent mechanism such as calcium leakage (JNK-AKT/mTOR signaling) [38]. Here, we demonstrate that verapamil enhanced IRE1- and PERK-mediated pathways, indicating that verapamil further activates the UPR and might trigger an autophagic, caspase-independent cell death. In the presence of the autophagy inhibitor 3-methyladenine, we observed a higher viability in verapamil-treated cells compared with cells cultured with verapamil alone (Figure W3), suggesting that verapamil-induced autophagy might contribute to cytotoxicity. Verapamil treatment also increased ROS production, leading to oxidative stress that was also shown to activate autophagy and mitochondrial dysfunction [39]. Mitochondrial ROS can further increase calcium release from the ER, thereby causing protein misfolding. ROS production and protein misfolding together activate calcium-dependent kinases such as JNK eventually leading to cell death [40]. Thus, we showed that verapamil supports bortezomib's ability to promote proapoptotic UPR signals such as CHOP induction and JNK activation. Bortezomib itself leads usually to a slight induction of NF- $\kappa$ B, presumably due to ER stress and consecutive UPR activation, which is not completely blocked by bortezomib-mediated inhibition of I $\kappa$ B degradation, as recently described by Hideshima et al. [41]. Remarkably, combination treatment with bortezomib and verapamil markedly inhibited the transcription factor NF- $\kappa$ B, a fact which might critically contribute to cell death induction in JK-6L cells. Moreover, autophagy-induced protein degradation could further decrease NF- $\kappa$ B activity [42].

Interference with MDR represents a further potential mechanism to increase cytotoxicity by the combination of the two drugs. Verapamil

functions as an inhibitor of drug efflux pump proteins such as the P-gp [15]. Many tumor cell lines overexpress drug efflux pumps, limiting the effectiveness of cytotoxic drugs. A recent study showed that efflux pump inhibitors enhanced the effect of bortezomib on drug-resistant Ewing tumors [43]. Using P-gp-positive and P-gp-negative cells, Rumpold et al. [44] provided evidence that bortezomib acts as a MDR1 substrate. We observed lower P-gp expression on JK-6L cells accompanied by impaired efflux of daunorubicin in cells treated with bortezomib/verapamil (data not shown), speculating that inhibition of P-gp might result in a reduced bortezomib efflux, leading to increasing amounts of intracellular bortezomib concentrations augmenting cell stress.

Approximately 60% of nonresistant JK-6L myeloma cells express P-gp on their surface. As expected, long-term culturing in the presence of bortezomib rendered these cells resistant to bortezomib, resulting in an increased P-gp expression (data not shown). These resistant JK-6L cells could be partially sensitized against bortezomib by verapamil (Figure W4). However, we assume that the increased sensitivity mainly results from UPR/stress-induced apoptosis and simultaneous inhibition of the antiapoptotic factor NF- $\kappa$ B, whereas the subtle MDR-mediated effects may play only a minor role. Further investigations are required to elucidate the exact mechanisms how verapamil triggers these signals.

In summary, our data provide a biochemical base for a new potential combination therapy of bortezomib together with verapamil, which should markedly enhance the killing of myeloma cells. Moreover, the efficiency of bortezomib treatment can be enhanced by the combination with verapamil. In addition, this drug combination may allow decreasing the bortezomib dose thereby reducing adverse effects. Animal experiments exploring the use of this combination treatment in myeloma models are underway.

## Acknowledgments

The authors thank Daniela Graef for technical assistance and Till T. Wisniewski for discussion (Department of Internal Medicine 1, University Hospital of Erlangen, Germany). The JK-6L cell line was kindly provided by Martin Gramatzki (Division of Stem Cell Transplantation, 2nd Department, University of Kiel, Germany). The RPMI 8226 and ARH-77 cell lines were a kind gift from the laboratory of Hans-Martin Jäck (Division of Molecular Immunology, Internal Medicine 3, University Erlangen, Germany).

## References

- [1] Kyle RA and Rajkumar SV (2008). Multiple myeloma. *Blood* **111**, 2962–2972.
- [2] Richardson PG, Mitsiades C, Hideshima T, and Anderson KC (2006). Bortezomib: proteasome inhibition as an effective anticancer therapy. *Annu Rev Med* **57**, 33–47.
- [3] Hideshima T, Richardson P, Chauhan D, Palombella VJ, Elliott PJ, Adams J, and Anderson KC (2001). The proteasome inhibitor PS-341 inhibits growth, induces apoptosis, and overcomes drug resistance in human multiple myeloma cells. *Cancer Res* **61**, 3071–3076.
- [4] Jackson G, Einsele H, Moreau P, and Miguel JS (2005). Bortezomib, a novel proteasome inhibitor, in the treatment of hematologic malignancies. *Cancer Treat Rev* **31**, 591–602.
- [5] Hershko A and Ciechanover A (1998). The ubiquitin system. *Annu Rev Biochem* **67**, 425–479.
- [6] Yang L, Carlson SG, McBurney D, and Horton WE Jr (2005). Multiple signals induce endoplasmic reticulum stress in both primary and immortalized chondrocytes resulting in loss of differentiation, impaired cell growth, and apoptosis. *J Biol Chem* **280**, 31156–31165.
- [7] Hayden MS and Ghosh S (2004). Signaling to NF- $\kappa$ B. *Genes Dev* **18**, 2195–2224.
- [8] Neubert K, Meister S, Moser K, Weisel F, Maseda D, Amann K, Wiethe C, Winkler TH, Kalden JR, Manz RA, et al. (2008). The proteasome inhibitor bortezomib

- depletes plasma cells and protects mice with lupus-like disease from nephritis. *Nat Med* **14**, 748–755.
- [9] Meister S, Schubert U, Neubert K, Herrmann K, Burger R, Gramatzki M, Hahn S, Schreiber S, Wilhelm S, Herrmann M, et al. (2007). Extensive immunoglobulin production sensitizes myeloma cells for proteasome inhibition. *Cancer Res* **67**, 1783–1792.
- [10] Obeng EA, Carlson LM, Gutman DM, Harrington WJ Jr, Lee KP, and Boise LH (2006). Proteasome inhibitors induce a terminal unfolded protein response in multiple myeloma cells. *Blood* **107**(12), 4907–4916.
- [11] Nawrocki ST, Carew JS, Pino MS, Highshaw RA, Dunner K Jr, Huang P, Abbruzzese JL, and McConkey DJ (2005). Bortezomib sensitizes pancreatic cancer cells to endoplasmic reticulum stress-mediated apoptosis. *Cancer Res* **65**, 11658–11666.
- [12] Gass JN, Gifford NM, and Brewer JW (2002). Activation of an unfolded protein response during differentiation of antibody-secreting B cells. *J Biol Chem* **277**, 49047–49054.
- [13] Patil C and Walter P (2001). Intracellular signaling from the endoplasmic reticulum to the nucleus: the unfolded protein response in yeast and mammals. *Curr Opin Cell Biol* **13**, 349–355.
- [14] Testa U (2009). Proteasome inhibitors in cancer therapy. *Curr Drug Targets* **10**, 968–981.
- [15] McTavish D and Sorkin EM (1989). Verapamil. An updated review of its pharmacodynamic and pharmacokinetic properties, and therapeutic use in hypertension. *Drugs* **38**, 19–76.
- [16] Muller C, Bailly JD, Goubin F, Laredo J, Jaffrezou JP, Bordier C, and Laurent G (1994). Verapamil decreases P-glycoprotein expression in multidrug-resistant human leukemic cell lines. *Int J Cancer* **56**, 749–754.
- [17] Schuh W, Meister S, Roth E, and Jack HM (2003). Cutting edge: signaling and cell surface expression of a  $\mu_H$  chain in the absence of  $\lambda_5$ : a paradigm revisited. *J Immunol* **171**, 3343–3347.
- [18] Frey B, Franz S, Sheriff A, Korn A, Bluemelhuber G, Gaipf US, Voll RE, Meyer-Pittroff R, and Herrmann M (2004). Hydrostatic pressure induced death of mammalian cells engages pathways related to apoptosis or necrosis. *Cell Mol Biol (Noisy-le-grand)* **50**, 459–467.
- [19] Piazza FA, Gurrieri C, Trentin L, and Semenzato G (2007). Towards a new age in the treatment of multiple myeloma. *Ann Hematol* **86**, 159–172.
- [20] Sun SC, Ganchi PA, Ballard DW, and Greene WC (1993). NF- $\kappa$ B controls expression of inhibitor I $\kappa$ B $\alpha$ : evidence for an inducible autoregulatory pathway. *Science* **259**, 1912–1915.
- [21] Todd DJ, Lee AH, and Glimcher LH (2008). The endoplasmic reticulum stress response in immunity and autoimmunity. *Nat Rev Immunol* **8**, 663–674.
- [22] Yoshida H, Matsui T, Yamamoto A, Okada T, and Mori K (2001). XBP1 mRNA is induced by ATF6 and spliced by IRE1 in response to ER stress to produce a highly active transcription factor. *Cell* **107**, 881–891.
- [23] Hetz C, Bernasconi P, Fisher J, Lee AH, Bassik MC, Antonsson B, Brandt GS, Iwakoshi NN, Schinzel A, Glimcher LH, et al. (2006). Proapoptotic BAX and BAK modulate the unfolded protein response by a direct interaction with IRE1 $\alpha$ . *Science* **312**, 572–576.
- [24] Puthalakath H, O'Reilly LA, Gunn P, Lee L, Kelly PN, Huntington ND, Hughes PD, Michalak EM, McKimm-Breschkin J, Motoyama N, et al. (2007). ER stress triggers apoptosis by activating BH3-only protein Bim. *Cell* **129**, 1337–1349.
- [25] Yoneda T, Imaizumi K, Oono K, Yui D, Gomi F, Katayama T, and Tohyama M (2001). Activation of caspase-12, an endoplasmic reticulum (ER) resident caspase, through tumor necrosis factor receptor-associated factor 2-dependent mechanism in response to the ER stress. *J Biol Chem* **276**, 13935–13940.
- [26] Mimnaugh EG, Xu W, Vos M, Yuan X, Isaacs JS, Bisht KS, Gius D, and Neckers L (2004). Simultaneous inhibition of hsp 90 and the proteasome promotes protein ubiquitination, causes endoplasmic reticulum-derived cytosolic vacuolization, and enhances antitumor activity. *Mol Cancer Ther* **3**, 551–566.
- [27] Kabeya Y, Mizushima N, Ueno T, Yamamoto A, Kirisako T, Noda T, Kominami E, Ohsumi Y, and Yoshimori T (2000). LC3, a mammalian homologue of yeast Apg8p, is localized in autophagosomal membranes after processing. *Embo J* **19**, 5720–5728.
- [28] Schubert U, Anton LC, Gibbs J, Norbury CC, Yewdell JW, and Bennink JR (2000). Rapid degradation of a large fraction of newly synthesized proteins by proteasomes. *Nature* **404**, 770–774.
- [29] Fekete MR, McBride WH, and Pajonk F (2005). Anthracyclines, proteasome activity and multi-drug-resistance. *BMC Cancer* **5**, 114.
- [30] Gulow K, Bienert D, and Haas IG (2002). BiP is feed-back regulated by control of protein translation efficiency. *J Cell Sci* **115**, 2443–2452.
- [31] Zhao Q, Wang J, Levichkin IV, Stasinopoulos S, Ryan MT, and Hoogenraad NJ (2002). A mitochondrial specific stress response in mammalian cells. *EMBO J* **21**, 4411–4419.
- [32] Urano F, Wang X, Bertolotti A, Zhang Y, Chung P, Harding HP, and Ron D (2000). Coupling of stress in the ER to activation of JNK protein kinases by transmembrane protein kinase IRE1. *Science* **287**, 664–666.
- [33] McCullough KD, Martindale JL, Klotz LO, Aw TY, and Holbrook NJ (2001). Gadd153 sensitizes cells to endoplasmic reticulum stress by down-regulating Bcl2 and perturbing the cellular redox state. *Mol Cell Biol* **21**, 1249–1259.
- [34] Masciarelli S, Fra AM, Pengo N, Bertolotti M, Cenci S, Fagioli C, Ron D, Hendershot LM, and Sitia R. (2010). CHOP-independent apoptosis and pathway-selective induction of the UPR in developing plasma cells. *Mol Immunol* **47**, 1356–1365.
- [35] Kim I, Xu W, and Reed JC (2008). Cell death and endoplasmic reticulum stress: disease relevance and therapeutic opportunities. *Nat Rev Drug Discov* **7**, 1013–1030.
- [36] Sun Y and Peng ZL (2009). Programmed cell death and cancer. *Postgrad Med J* **85**, 134–140.
- [37] Williams A, Sarkar S, Cudon P, Trofi EK, Saiki S, Siddiqi FH, Jahreis L, Fleming A, Pask D, Goldsmith P, et al. (2008). Novel targets for Huntington's disease in an mTOR-independent autophagy pathway. *Nat Chem Biol* **4**, 295–305.
- [38] Ding WX and Yin XM (2008). Sorting, recognition and activation of the misfolded protein degradation pathways through macroautophagy and the proteasome. *Autophagy* **4**, 141–150.
- [39] Zhang K and Kaufman RJ (2008). From endoplasmic-reticulum stress to the inflammatory response. *Nature* **454**, 455–462.
- [40] Malhotra JD and Kaufman RJ (2007). Endoplasmic reticulum stress and oxidative stress: a vicious cycle or a double-edged sword? *Antioxid Redox Signal* **9**, 2277–2293.
- [41] Hideshima T, Ikeda H, Chauhan D, Okawa Y, Raje N, Podar K, Mitsiades C, Munshi NC, Richardson PG, Carrasco RD, et al. (2009). Bortezomib induces canonical nuclear factor- $\kappa$ B activation in multiple myeloma cells. *Blood* **114**, 1046–1052.
- [42] Xiao G (2007). Autophagy and NF- $\kappa$ B: fight for fate. *Cytokine Growth Factor Rev* **18**, 233–243.
- [43] Nakamura T, Tanaka K, Matsunobu T, Okada T, Nakatani F, Sakimura R, Hanada M, and Iwamoto Y (2007). The mechanism of cross-resistance to proteasome inhibitor bortezomib and overcoming resistance in Ewing's family tumor cells. *Int J Oncol* **31**, 803–811.
- [44] Rumpold H, Salvador C, Wolf AM, Tilg H, Gastl G, and Wolf D (2007). Knockdown of PgP resensitizes leukemic cells to proteasome inhibitors. *Biochem Biophys Res Commun* **361**, 549–554.

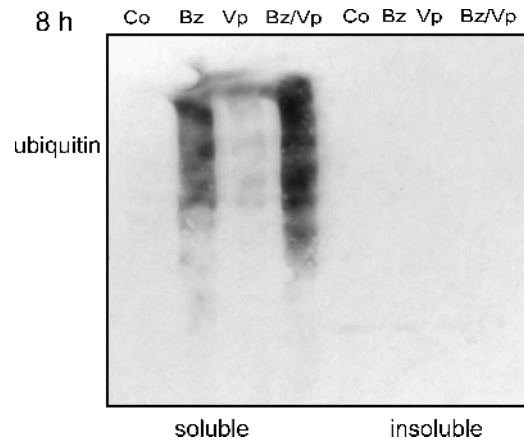


**Figure W1.** Combination treatment of bortezomib and verapamil for 8 hours resulted in the accumulation of ubiquitinated proteins in soluble fractions. Western blot analysis of detergent-soluble and detergent-insoluble fractions of JK-6L cells treated with 10 nM bortezomib and/or 70  $\mu$ M verapamil for 8 hours. Immunoblot analysis was done using an antiubiquitin antibody. One representative immunoblot of two independent experiments is shown. *Bz* indicates bortezomib; *Co*, control (PBS-treated); *Vp*, verapamil.

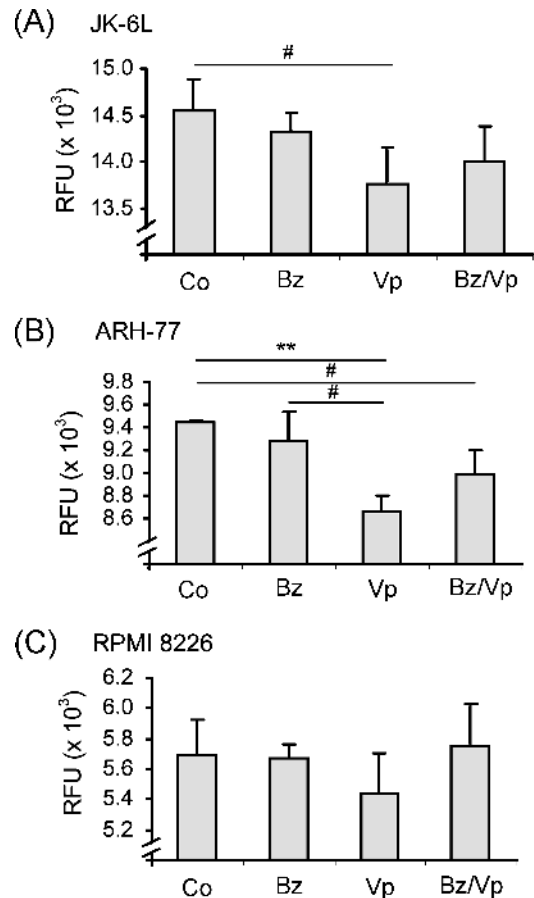


**Figure W2.** The intracellular calcium level was diminished by verapamil in myeloma cell lines. (A–C) Myeloma cells ( $1 \times 10^6$ ) were treated with 10 nM bortezomib and/or 70  $\mu$ M verapamil for 2 hours. To evaluate the cellular  $\text{Ca}^{2+}$  flux, cells were harvested by centrifugation and resuspended with 0.8 ml of Fluo-8 NW dye-loading solution from the Screen Quest Fluo-8 NW Calcium Assay Kit (ATT Bioquest Inc, Sunnyvale, CA). The cell suspension was plated 100  $\mu$ l per well in a 96-well black well plate (Nunc; Thermo Fisher Scientific) precoated with poly-L-lysine (Sigma). The plates were incubated at 37°C for 30 minutes and then placed at room temperature for another 30 minutes. Fluorescence at Ex = 485 nm/Em = 535 nm was measured by a bioassay reader (HTS 7000; PerkinElmer, Waltham, MA) and depicted as relative fluorescence units (RFUs). Mean values and SD were calculated from triplicates. Data represent one of three independently done experiments. Student's *t*-test for unpaired heteroscedastic samples was used for statistical analysis. #*P* < .05, \**P* < .01, \*\**P* < .001, \*\*\**P* < .0001. *Bz* indicates bortezomib; *Co*, control (PBS-treated); *Vp*, verapamil.

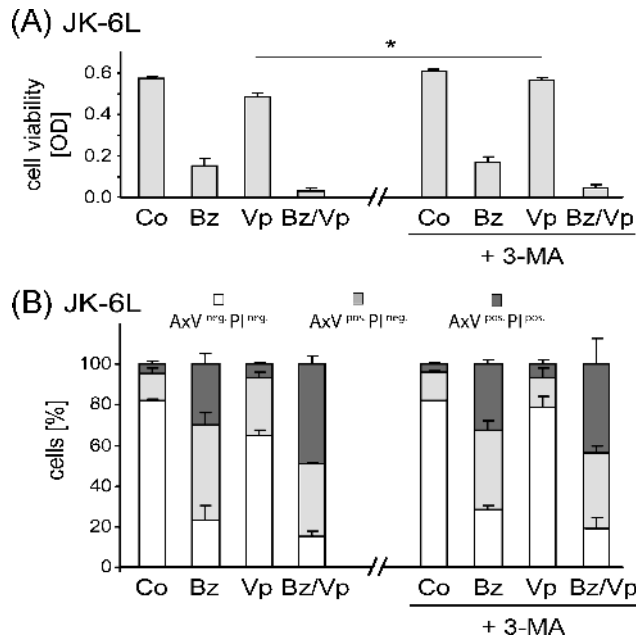


**Figure W3.** The reduced viability of verapamil-treated cells was slightly reverted by the autophagy inhibitor 3-methyladenine. JK-6L cells were treated with 10 nM bortezomib and 70  $\mu$ M verapamil or the combination of both inhibitors in the absence or presence of 1 mM 3-methyladenine for 16 hours. (A) Cells were incubated with the vital dye AlamarBlue. The absorbance (OD) was measured using a spectrophotometer. Only relevant significance values are depicted. (B) The diagram shows the percentages of viable (annexin V-FITC<sup>negative</sup>/propidium iodide<sup>negative</sup>), apoptotic (annexin V-FITC<sup>positive</sup>/propidium iodide<sup>negative</sup>), and necrotic/late apoptotic (annexin V-FITC<sup>positive</sup>/propidium iodide<sup>positive</sup>) cells, analyzed by flow cytometry. Mean values and SD were calculated from triplicates. Data represent one of three independently done experiments. Student's *t*-test for unpaired heteroscedastic samples was used for statistical analysis. #*P* < .05, \**P* < .01, \*\**P* < .001, \*\*\**P* < .0001. 3-MA indicates 3-methyladenine; AxV, annexin V-FITC; Bz, bortezomib; Co, control (H<sub>2</sub>O-treated); PI, propidium iodide; Vp, verapamil.

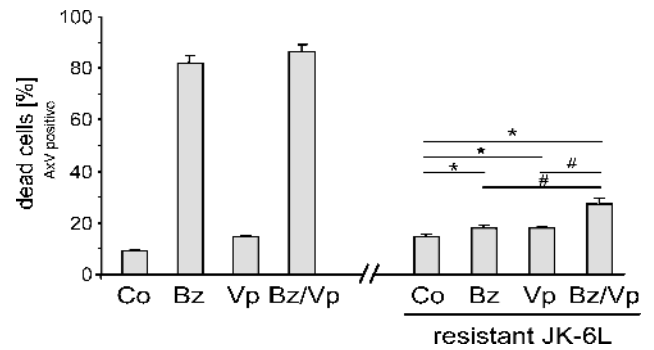


**Figure W4.** Bortezomib together with verapamil enhanced the cytotoxic activity toward bortezomib-resistant JK-6L cells. JK-6L cells were cultured during three months with 10 nM bortezomib to establish bortezomib-resistant cells. Nonresistant and resistant JK-6L cells were treated with 10 nM bortezomib and 70  $\mu$ M verapamil or the combination of both inhibitors for 16 hours. The diagram shows the percentages of dead (annexin V-FITC<sup>positive</sup>) cells analyzed by flow cytometry. Mean values and SD were calculated from triplicates. Data represent one of three independently done experiments. Only relevant significance values are depicted. Student's *t*-test for unpaired heteroscedastic samples was used for statistical analysis. #*P* < .05, \**P* < .01, \*\**P* < .001, \*\*\**P* < .0001. AxV indicates annexin V-FITC; Bz, bortezomib; Co, control (PBS-treated); Vp, verapamil.